Geometric nonlinear dynamic analysis of uncertain structures with cyclic symmetry - Application to a mistuned industrial bladed disk

Evangéline Capiez-Lernout, Christian Soize, M. Mbaye

In the proceedings of the international conference USD 2014, Katholieke Universiteit Leuven, Belgium, September 15-17, 2014

Geometric nonlinear dynamic analysis of uncertain structures with cyclic symmetry. Application to a mistuned industrial bladed disk.

E. Capiez-Lernout [1], **C. Soize** [1], **M. Mbaye** [2]
[1] Université Paris-Est, Laboratoire Modélisation et Simulation Multi-échelle,
MSME UMR 8208 CNRS, 5 bd Descartes, 77454 Marne-la-Vallée Cedex 02, France
e-mail: **evangeline.capiez-lernout@u-pem.fr**

[2] SAFRAN Turbomeca, 64511 Bordes

Abstract
This paper deals with the dynamical analysis of a mistuned industrial rotating integrally bladed disk, for which the operating regime under consideration takes into account the nonlinear geometrical effects induced by large displacements and deformations. First, a dedicated mean nonlinear reduced-order model of the tuned structure is explicitly constructed using the finite element method. The random nature of the mistuning is then modeled by using the nonparametric probabilistic approach extended to the nonlinear geometric context. The capability of the methodology to be applied to realistic industrial models is demonstrated through the paper. The dynamic analysis of the random response is then conducted in the frequency domain in order to quantify the impact of the nonlinear geometrical effects on the mistuned structure.

1 Introduction

In general, the natural cyclic symmetry of turbomachinery bladed disks is broken because of manufacturing tolerances and material dispersions, which create small variations from one blade to another one. Such phenomena, referred to mistuning, can generate localization effects combined to a dynamic amplification of the forced response [1]. Many research efforts have been carried out on this subject, including reduced-order models with probabilistic approaches in the numerical modeling, for taking into account the random character of mistuning [2, 6, 3] and giving rise to strategies for the robust design of such structures [4, 5]. Another essential aspect is to consider the geometrically nonlinear effects in the computational models occurring when exceptional operating speeds of bladed disks are analyzed due to geometric nonlinearities induced by large deformations and large displacements [7, 8]. Such situation is realistic when considering a flutter kind phenomenon induced by unsteady aerodynamic coupling and yielding low damping levels. Since the unsteady aerodynamic coupling is not considered in this paper, the nonlinear domain is simulated by increasing the magnitude of the external load, while performing forced response calculations.

The present paper proposes a methodology adapted to geometric nonlinear analysis of mistuned bladed disks combined with an industrial realistic application. The first part is devoted to the development of an adapted nonlinear reduced-order computational model for the tuned structure, referred as the mean NL-ROM. It is explicitly constructed in the context of three-dimensional solid finite elements [9] by using an appropriate projection basis [10] obtained here by a linear tuned eigenvalue analysis. Once the mean NL-ROM is established, mistuning is taken into account by implementing uncertainties through the nonparametric probabilistic framework [11, 12].

The paper is organized as follows. Section 2 describes the computational methodology and the computational aspects allowing the nonlinear dynamic analysis of mistuned rotating bladed-disks to be performed. Section 3 is devoted to the application, consisting of a finite-element model of an industrial integrated bladed disk with about 2, 000, 000 dof. The geometrically nonlinear effects are analyzed and quantified through the dynamic analysis of the magnification factor in both tuned and mistuned cases.

2 Methodology

This Section is devoted to the construction of a methodology for the nonlinear mistuning analysis occurring in rotating bladed-disks structures. In the present research, the bladed-disks under consideration are assumed (1) to be made up of a linear elastic material and (2) to undergo large displacements and large deformations inducing geometrical nonlinearities.

Nonlinear dynamics of a tuned bladed-disk

The tuned bladed-disk structure has an N-order cyclic symmetry. Thus, the geometrical domain, the material constitutive equation and the boundary conditions related to the generating sector are invariant under the $2\pi/N$ rotation around its axis of symmetry. Moreover, the bladed disk undergoes a rotational motion around the axis of symmetry with constant angular speed Ω. A total Lagrangian formulation is chosen, which means that the dynamical equations are expressed in the rotating frame of an equilibrium configuration considered as a prestressed static configuration.

The mean (or nominal) computational model of the tuned bladed-disk, which is constructed by the finite element method (FEM) is written as

$$\begin{aligned} [M]\,\ddot{\mathbf{u}} + ([C(\Omega)] + [D])\,\dot{\mathbf{u}} + [K(\Omega)]\,\mathbf{u} + \mathbf{f}^{NL}(\mathbf{u}) &= \mathbf{f} \quad , \\ [K(\Omega)] &= [K_e] + [K_g] + [K_c(\Omega)] \quad , \end{aligned} \tag{1}$$

in which the $\mathbb{R}^n$-vector $\mathbf{f}$ corresponds to the finite element discretization of the external force fields, which are derived from the Lagrangian transport into the reference configuration of the physical body/surface force fields applied in the deformed configuration. The external load can represent, for instance, the unsteady pressures applied to the blades. In Eq. (1), the $\mathbb{R}^n$-vector $\mathbf{u}$ corresponds to the finite element discretization of the unknown displacement field expressed with respect to the reference configuration. In Eq. (1), the matrices $[M]$, $[D]$, $[K_g]$ and $[K_e]$ are the mass, damping, geometrical stiffness and elastic stiffness real matrices with positive definiteness property. The rotational effects are taken into account through the gyroscopic coupling matrix $[C(\Omega)]$ and the centrifugal stiffness matrix $[K_c(\Omega)]$, with antisymmetry property and with negative definiteness property respectively. It should be noted that all these matrices are also N-block circulant matrices since the structure has an N-order cyclic symmetry. The geometrical nonlinearities effects are taken into account through the $\mathbb{R}^n$-vector $\mathbf{f}^{NL}(\mathbf{u})$ which includes both quadratic and cubic stiffness terms. Furthermore, the centrifugal effects are assumed to be sufficiently small so that the linear stiffness matrix $[K(\Omega)]$ is positive definite, yielding only stable dynamical systems to be considered.

In the present case, the presence of the geometric nonlinearity naturally yields the nonlinear equations to be solved in the time domain, the frequency content of the nonlinear response being *a posteriori* post-analyzed by Fourier transform. The external load is defined in the time domain corresponding to a uniform sweep of a chosen frequency band of excitation. Let $\widetilde{\mathbb{B}}_s = -\mathbb{B}_s \cup \mathbb{B}_s$ be the frequency band of excitation with central frequency $s\Delta\,\omega$ and bandwidth $\Delta\omega$ defined by $\mathbb{B}_s = [(s-1/2)\Delta\omega, (s+1/2)\Delta\omega]$. The external load is written as

$$\mathbf{f}(t) = f_0\, g(t)\, \boldsymbol{\alpha} \quad , \tag{2}$$

in which f_0 is a coefficient characterizing the global load intensity, and where $\boldsymbol{\alpha}$ is an $\mathbb{R}^n$-vector corresponding to the spatial discretization of the load. In Eq. (2), the function $g(t)$ is chosen as

$$g(t) \;=\; \frac{\Delta\omega}{\pi} sinc_{\pi}(\frac{t\Delta\omega}{2\pi})\,\cos(s\,\Delta\omega\,t) \quad , \tag{3}$$

where $x \mapsto sinc_{\pi}(x)$ is the function defined by $sinc_{\pi}(x) \;=\; sin(\pi\,x)/(\pi\,x)$. It should be noted that all the frequencies of the frequency band of excitation are simultaneously excited so that only one nonlinear time-domain analysis is carried out. With such time-domain excitation, a forced-response problem is considered and not a time evolution problem with initial conditions. The considered forced-response problem is thus approximated by an equivalent time-evolution problem with zero initial conditions over a finite time interval, which includes almost all of the signal energy of the excitation. The use of the cyclic symmetry property by decomposing the nonlinear response according to its harmonic components is not considered because all the harmonic components are coupled through the geometric nonlinearity, and does not allow the problem on a single generator sector to be solved. Moreover, the full computation of the nonlinear solution of Eq. (1) induces a large computational effort, when dealing with realistic models of bladed-disks corresponding to a large number of DOF. Consequently, for large computational models, a reduced-order model strategy is used, and is adapted to the geometric nonlinear context under consideration (see [13, 14, 9] and [10] for a complete overview). Let a given vector basis be represented by the $(n \times P)$ real matrix $[\Phi]$. The nonlinear response $\mathbf{u}$ is expanded as

$$\mathbf{u} \;=\; [\Phi]\,\mathbf{q} \quad , \tag{4}$$

in which $\mathbf{q}$ is the $\mathbb{R}^P$-vector of the generalized coordinates. Replacing Eq. (4) into Eq. (1) yields a nonlinear reduced set of P coupled differential equations for which all linear, quadratic and cubic terms have to be known. In the present research, the construction of the operators of such mean nonlinear reduced-order model (mean NL-ROM) is explicitly carried out in the context of the three-dimensional finite element method. It is assumed that the finite elements are isoparametric solid finite elements with 8 nodes, and using a numerical integration with 8 Gauss integration points. The elementary internal forces projected on the chosen vector basis are numerically constructed for each finite element before performing its assembly and computing all linear and nonlinear reduced operators. The detailed procedure, which also uses the symmetry properties of the linear and nonlinear reduced operators combined with distributed computations, can be found in [14]. It should be noted that each type of reduced operator is separately modeled, keeping open the possibility of implementing uncertainties issued from independent physical sources.

Nonlinear analysis of a mistuned bladed-disk

The random nature of the mistuning is then considered by implementing the nonparametric probabilistic approach, which presents the ability to include both the system-parameter uncertainties and the model uncertainties induced by modeling errors (see [11] for a complete review on the subject). It consists in replacing the operators of the mean NL-ROM by random operators, whose probability distribution is derived from the maximum entropy principle.

Let $[\mathcal{A}]$ be a $(Q \times Q)$ matrix issued from the mean NL-ROM. The corresponding random matrix $[\boldsymbol{\mathcal{A}}]$ is then written as $[\boldsymbol{\mathcal{A}}] \;=\; [U_A]\,[L_A]^T\,[\mathbf{G}_A]\,[L_A]$, where $[\mathbf{G}_A]$ is a $(Q \times Q)$ random positive-definite matrix whose probability model is issued from the MaxEnt principle [12]. When $[\mathcal{A}]$ is a mean reduced operator with positive-definite property, representing either the mass, damping, geometrical stiffness or the opposite of the centrifugal stiffness, we have $Q \;=\; P$. When $[\mathcal{A}]$ is the mean reduced positive-definite operator issued from the reshaping of the linear elastic, quadratic and cubic stiffness as shown in [15], we have $Q \;=\; P(P+1)$. For these cases the $(Q \times Q)$ matrix $[L_A]$ is issued from the Cholesky factorization of $[\mathcal{A}]$ and matrix $[U_A]$ is the $(Q \times Q)$ identity matrix. When $[\mathcal{A}]$ is a mean reduced operator with antisymmetry property such that the gyroscopic coupling matrix, the matrices $[U_A]$ and $[L_A]$ are the $(P \times P)$ matrices defined by $[L_A] \;=\; [S_A]^{1/2}\,[B_A]^T$ and $[U_A] \;=\; [\mathcal{A}]\,[B_A]\,[S_A]\,[B_A]^T$, in which the $(P \times P)$ full and diagonal matrices $[B_A]$ and $[S_A]$ are issued from the single value decomposition (SVD) of operator $[\mathcal{A}]$. The dispersion of each random operator is then characterized by one scalar hyperparameter. Consequently, the mistuning

level of the bladed-disk is entirely controlled by the $\mathbb{R}^6$-vector $\boldsymbol{\delta} = (\delta_M, \delta_D, \delta_C, \delta_{K_g}, \delta_{K_c}, \delta_K)$, belonging to an admissible set.

Numerical computations

The solution of the stochastic NL-ROM is calculated using the Monte Carlo numerical simulation. For each realization, a set of P nonlinear coupled differential equations is considered and solved with the Newmark method, for which the averaging acceleration scheme, known to be unconditionally stable is used. With this solver, a set of nonlinear equations whose solution is denoted by the $\mathbb{R}^P$-vector $\mathbb{q}$ has to be solved at each sampling time. Such computation is mainly addressed by the fixed point method because the iterative scheme does not require the evaluation of the tangential stiffness matrix. Nevertheless, when the algorithm does not converge, it is replaced by the Crisfield arc-length method [16]. Such algorithm introduces an additional scalar unknown $\mathbb{\mu}$ that multiplies the right-hand side member of the nonlinear equation. It is solved step by step, each incremental step being characterized by a given arc length. For a given step, an iterative scheme requiring one evaluation of the tangential stiffness matrix allows a solution $(\mathbb{q}, \mathbb{\mu})$ to be computed. An adaptive arc length, depending on the number of iterations necessary to obtain the convergence of the preceding increment is also implemented. Furthermore, since parameter $\mathbb{\mu}$ has to be controlled to be equal to 1, the state of the algorithm corresponding to the preceding increment has to be stored. Even if the procedure is time consuming, its main advantage concerns its capability of capturing high-nonlinear mechanical behaviors.

3 Application to an industrial bladed-disk

Nonlinear deterministic analysis

Description of the external load

The structure under consideration in an industrial turbine geometry belonging to the class of integrated bladed disks. Due to proprietary reasons, the number N of blades characterizing the order of the cyclic symmetry of the structure is not given. The finite element model of the structure is constructed with solid finite elements and is constituted of about $2\,000\,000$ degrees of freedom. Fig. 1 displays a part of the finite element mesh of the investigated bladed disk. The structure is in rotation around its revolution axis with a constant velocity $\Omega = 30,750\,rpm$. Since the dynamic analysis is carried out in the rotating frame of the structure, the rigid body motion due to the rotation of the structure corresponds to a fixed boundary condition at the inner radius of the structure. The bladed disk is made up of a homogeneous isotropic material. An hysteretic damping model is added for the bladed disk.

Figure 1: Finite element mesh of a part of the structure

The cyclic symmetry is first used for constructing the reduced matrices of the mean linear reduced-order model (mean L-ROM). The linear generalized eigenvalue problem related to the tuned bladed-disk is then solved using this cyclic symmetry property [18, 19]. Let ν_0 be the first eigenfrequency. Figure 2 displays the dimensionless eigenfrequencies ν_i/ν_0 of the tuned structure with respect to the circumferential wave number n. The graph is truncated to $n = 5$ because a $5\,th$ engine-order excitation is presently considered around a veering corresponding to the dimensionless frequency excitation band $\mathbb{B}_e = [1.78\,,\,2.34]$.

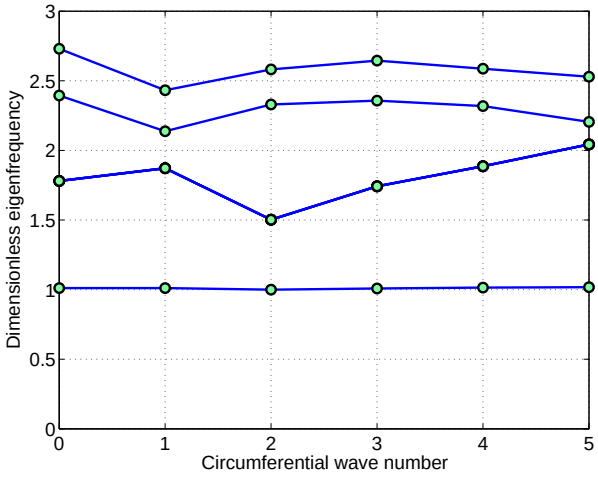

Figure 2: Natural frequencies with respect to circumferential wave number

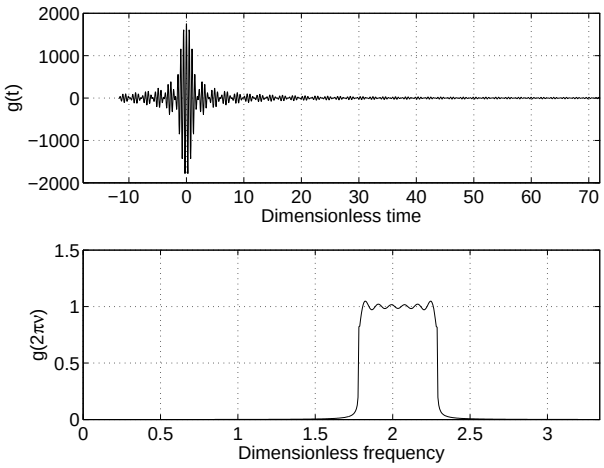

Figure 3: Representation of the external load in the time domain and in the frequency domain: graph of $t/t_0 \mapsto g(t)$ (upper graph) and $\nu/\nu_0 \mapsto \hat{g}(2\pi\nu)$ (lower graph) for $\mathbb{B}_e = [1.78\,,\,2.34]$.

Such excitation band of analysis is chosen through the time domain function $g(t)$ according to Eq. (2) such that $s = 4$ and $\Delta\omega/(2\pi\nu_0) = 0.5086$. The spatial distribution of the load is only concerned with point excitations located at the tip of each blade along the axial direction. Concerning the numerical sampling, the initial instant of integration t_{ini} and the total time duration T are chosen according to [17] such that $\nu_0\, t_{ini} = -11.79$ (corresponding to a zero value of function $g(t)$) and $\nu_0\, T = 184$. Figure 3 shows the graphs $\nu_0\, t \mapsto g(t)$ and $\nu/\nu_0 \mapsto \hat{g}(2\pi\nu)$. It should be noted that when only the tuned linear case is considered, there are only contributions on the $5-th$ circumferential wave number. The external load is fixed with $f_0 = 2.5\,N$, which corresponds to an high rate of geometrical nonlinearity. Such high loading can be interpreted as equivalent to a situation for which the damping of the bladed disk structure would reach

very small values. Such extreme situations are realistic when approaching flutter regimes. The frequency band of analysis is a broad frequency band corresponding to the dimensionless frequency band of analysis $\mathbb{B} = [0\,,\,3.34]$. The Shannon theorem is carried out with a higher sample frequency $\nu_e/\nu_0 = 11.12$, yielding the number n_t of time steps to be $n_t = 4,096$. The frequency resolution is then $\nu/\nu_0, = 0.0054$. Let $\hat{g}(2\pi\nu)$ be the Fourier transform of function $g(t)$. Figure 3 shows the graphs $t/t_0 \mapsto g(t)$ and $\nu/\nu_0 \mapsto \hat{g}(2\pi\nu)$.

Nonlinear tuned analysis

Concerning the choice of the vector basis for the construction of the mean NL-ROM, the nonlinear equations are solved in the subspace spanned by the usual linear basis constituted of the P modal shapes related to the first increasing natural eigenfrequencies, according to [14]. A convergence analysis is carried out by increasing the size P of the reduced-order model. It can be shown that $P = 65$ yields a reasonable convergence. From now on, the converged solution corresponding to the observation issued from the mean NL-ROM is denoted by $\widetilde{\mathbf{u}}(t)$. For clarity, when confusion is possible, superscripts L and NL will be added for distinguishing the linear case from the geometric nonlinear one.

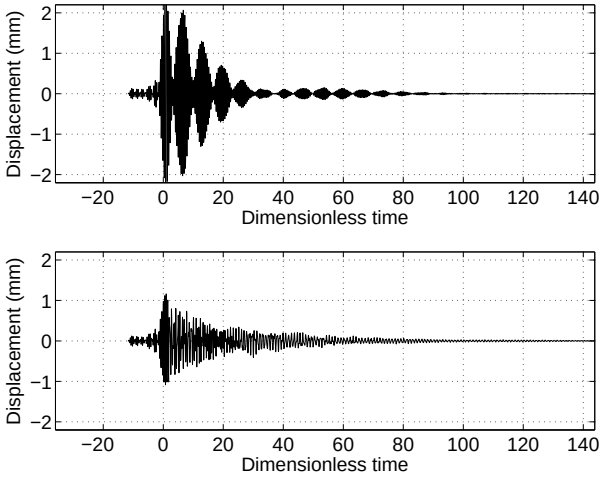

Figure 4: Time domain observation $t/t_0 \mapsto v(t)$ related to the linear (upper graph) and the nonlinear (lower graph) cases for $\mathbb{B}_e = [1.78\,,\,2.34]$.

Being interested in the blade yielding the highest vibration amplitude, let $j_0 = \arg\max_j \left(\max_t \widetilde{u}_j^{NL}(t)\right)$ The observation $v(t)$ corresponding to the selected blade out-plane displacement is defined by $v(t) = \widetilde{u}_{j_0}(t)$. Figure 4 displays the graph $t/t_0 \mapsto v^L(t)$ (upper graph) and $t/t_0 \mapsto v^{NL}(t)$ (lower graph). On these graphs, significant level of geometrical nonlinear effect can be observed. On this figure, it is seen that the geometric nonlinearities induce a blade stiffening characterized by a reduction of the vibration amplitudes of the blades from $2\,mm$ until $1\,mm$ with respect to the linear case. This stiffening is also combined with a strong irregularity of the blade response shape over time, which shows an enrichment of the frequency content, which has to be quantified.

Let $k_0 = \arg\max_j \left(\max_{\nu/\nu_0 \in \mathbb{B}} \widehat{\widetilde{u}}_j^{NL}(2\pi\nu)\right)$ for which $\widehat{\widetilde{u}}_j^{NL}(2\pi\nu)$ is the Fourier transform of $\widetilde{u}_j^{NL}(t)$. In the frequency domain, the observation $w(2\pi\nu)$ corresponding to the selected blade out-plane displacement is defined by $w(2\pi\nu) = \widehat{\widetilde{u}}_{k_0}(2\pi\nu)$. Figures 5 displays the graphs $\nu/\nu_0 \mapsto w^L(2\pi\nu)$ (upper graph) and $\nu/\nu_0 \mapsto w^{NL}(2\pi\nu)$ (lower graph). As expected, it can be seen that the frequency content of the blade response issued from the linear NL-ROM coincides with $\mathbb{B}_e$. The coupling issued from the strong nonlinear geometric effects is characterized through secondary response peaks, whose frequency content enlarges with increasing load rate. It should be noted that there also exist higher frequencies excited through this nonlinearity which are of less importance in the chosen band of analysis $\mathbb{B}$. As observed on the graphs, the amplitude

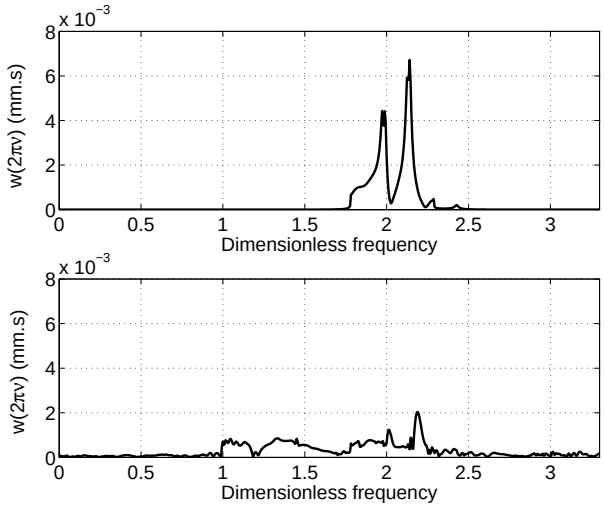

Figure 5: Frequency domain observation $\nu/\nu_0 \mapsto w(2\pi\nu)$ related to the linear (upper graph) and the nonlinear (lower graph) cases for $\mathbb{B}_e = [1.78\,,\,2.34]$.

levels from linear and nonlinear cases differ by a factor of about 3.5 for the main resonance. Concerning the nonlinear case, the secondary resonances occurring in the lower frequency range are in the same order of magnitude as the main resonance.

Nonlinear analysis of the mistuned bladed disk

In the present case, the mean NL-ROM is constructed by modal analysis without substructuring techniques. Thus, the uncertainties are not considered as independent from one blade to another one, which is coherent with the structure under consideration belonging to the class of integrated bladed disks, which are manufactured from a unique solid piece of material. In the present analysis, for a better understanding of the phenomenon, only the nonlinear part of the operators are considered to be deterministic. The mistuning level is thus controlled by the $\mathbb{R}^5$-vector $\boldsymbol{\delta} = (\delta_M, \delta_D, \delta_C, \delta_{K_c}, \delta_K)$.

Sensitivity analysis according to the type of uncertainties

The mistuning analysis is carried out in the frequency domain, requiring a Fourier transform of the observation. First, a sensitivity analysis is conducted in order to identify the dispersion parameters yielding the most significant effects on the mistuned response represented by the random variable $W(2\pi\nu)$ similar to observation $w(2\pi\nu)$ in the tuned case. As expected for the linear mistuned case, it can be observed that an uncertainty level of 0.1 for the gyroscopic coupling, or/and the centrifugal stiffness or/and the dissipation terms, has a very limited impact on the mistuned linear response. Thus, the mistuned linear response can be reasonably considered only sensitive to mass and elastic stiffness uncertainties.

Nevertheless, as shown in Figures 6 and 8, corresponding to the confidence region of observations $W^{NL}(2\pi\nu)$ and $W^{L}(2\pi\nu)$ with a probability level set to 0.95, the nonlinear mistuned behavior is shown to be substantially different. On one side, the nonlinear mistuned response behaves almost like its tuned counterpart for the frequency band of analysis corresponding to the frequency band of excitation. On the other side, the uncertainties spread throughout the geometrical nonlinearities, yielding large confidence regions for the nonlinear mistuned response in $\mathbb{B}\backslash\mathbb{B}_e$, more particularly in the dimensionless subfrequency range $\mathbb{B}_s = [1\,,\,1.2]$.

In Figure 6, corresponding to the case of uncertain gyroscopic coupling, the dynamical analysis in $\mathbb{B}_s$ shows realizations with amplification levels around 2 whereas the mistuned response remains unchanged in the

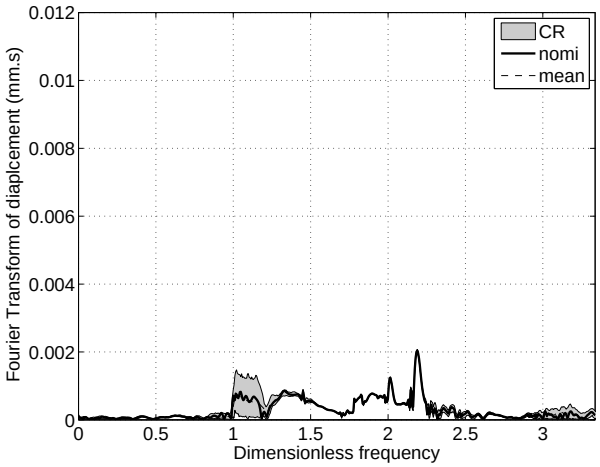

Figure 6: Stochastic analysis: frequency domain observation related to the nonlinear case when $\delta_C = 0.1$: mean model (thick line), mean of the stochastic model (thin dashed line), confidence region (gray region).

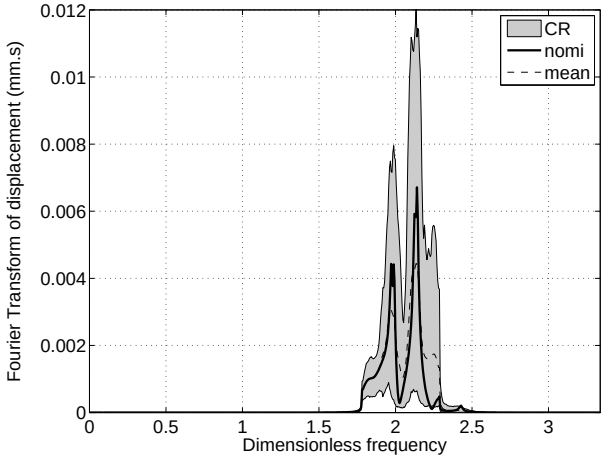

Figure 7: Stochastic analysis: frequency domain observation related to the linear case when $\delta_M = 0.1$: mean model (thick line), mean of the stochastic model (thin dashed line), confidence region (gray region).

excitation frequency band. Note that a similar nonlinear mistuned behavior can be observed for the cases of uncertain centrifugal stiffness or uncertain dissipation. By comparing Figures 7 and 8 corresponding to the linear and nonlinear cases in presence of mass uncertainty, it can be seen that the usual mistuning effects yielding a consequent dynamical amplification for the linear mistuned case, are strongly inhibited in $\mathbb{B}_e$ for the nonlinear mistuned case yielding amplification levels of magnitude 1.2. A wide spread of uncertainties is observed in $\mathbb{B}\backslash\mathbb{B}_e$ with amplification levels of magnitude 2.5 with respect to subfrequency band $\mathbb{B}_{sub} = [1\,,\,1.6]$. Such amplification levels yield similar response level than the nonlinear tuned response located in $\mathbb{B}_e$. Note that a similar behavior is observed for the case of elastic stiffness uncertainties.

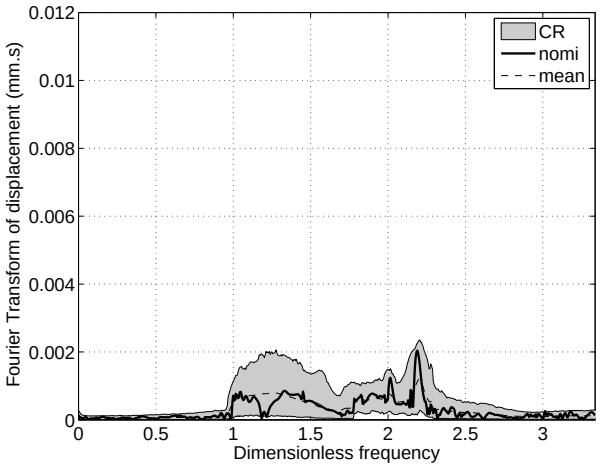

Figure 8: Stochastic analysis: frequency domain observation related to the linear case when $\delta_M = 0.1$: mean model (thick line), mean of the stochastic model (thin dashed line), confidence region (gray region).

Nonlinear dynamical analysis of the mistuned response

From now on, the uncertainty level is such that $\boldsymbol{\delta} = (\delta_M, \delta_D, \delta_C, \delta_{K_c}, \delta_K) = (\delta, 0.2, 0.2, 0.2, \delta)$. A parametric analysis according parameter δ is carried out in order to establish a comparison of the mistuning effects between the linear and the nonlinear mistuned cases. For fixed $\nu/\nu_0 \in \mathbb{B}$, let $Y(2\pi\nu)$ be the random dynamic observation defined by

$$Y(2\pi\nu) = \frac{W(2\pi\nu)}{\max_{\nu/\nu_0 \in \mathbb{B}} w(2\pi\nu)} \quad . \tag{5}$$

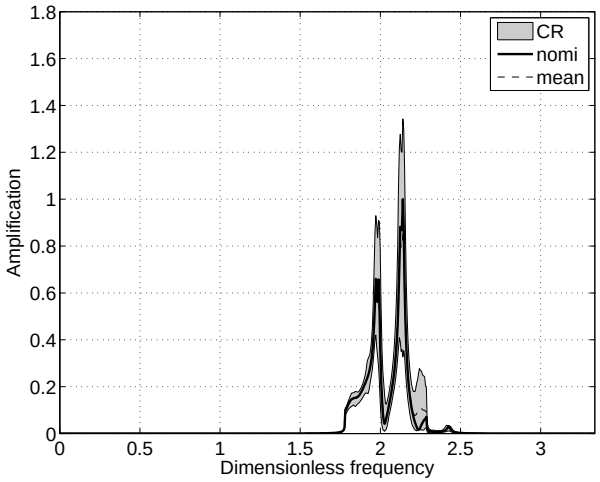

Figure 9: Stochastic analysis: frequency domain observation $Y^L(2\pi\nu)$ related to the linear case when $\delta_K = \delta_M = 0.02$ and $\delta_{K_c} = \delta_C = \delta_D = 0.2$: mean model (thick line), mean of the stochastic model (thin dashed line), confidence region (gray region).

Figures 9 (or 11) and 10 (or 12) show the confidence region of the linear and nonlinear observations $Y^L(2\pi\nu)$ and $Y^{NL}(2\pi\nu)$ when $\delta = 0.02$ (or $\delta = 0.16$). Those graphs allows the effects of mass and elastic uncertainties in presence of uncertainties issued from the rotational effects to be analyzed.

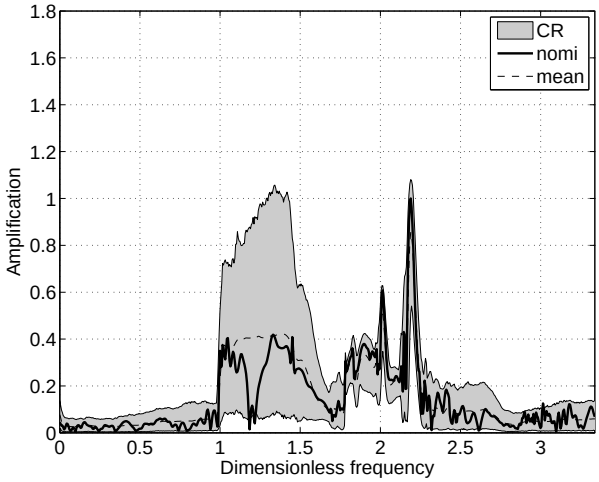

Figure 10: Stochastic analysis: frequency domain observation $Y^{NL}(2\pi\nu)$ related to the nonlinear case when $\delta_K = \delta_M = 0.02$ and $\delta_{K_c} = \delta_C = \delta_D = 0.2$: mean model (thick line), mean of the stochastic model (thin dashed line), confidence region (gray region).

For frequency band $\mathbb{B}_e$, it can be observed that an increase of the mistuning yields a uniform spread in the frequency domain around the main resonance, yielding a weak robustness with respect to uncertainties. It is also clearly seen that the linearized assumption tends to increase the extreme values of the response levels. The geometric nonlinear effects clearly inhibit the amplification of the random response. More particularly, the extreme values related to $Y^{NL}(2\pi\nu)$ yield moderate amplification even if the confidence region remain relatively broad.

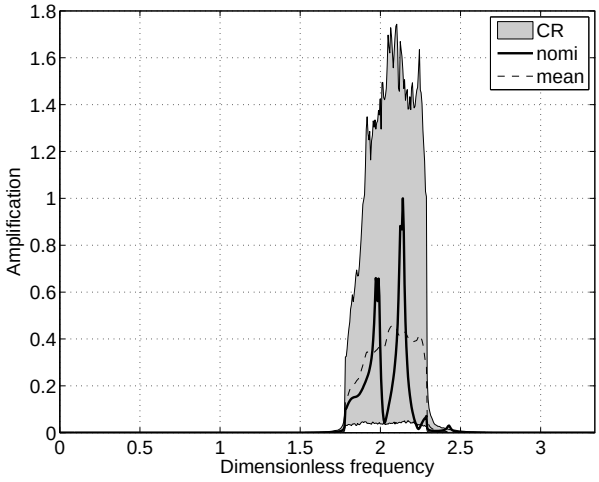

Figure 11: Stochastic analysis: frequency domain observation related to the linear case $Y^{L}(2\pi\nu)$ when $\delta_K = \delta_M = 0.16$ and $\delta_{K_c} = \delta_C = \delta_D = 0.2$: mean model (thick line), mean of the stochastic model (thin dashed line), confidence region (gray region).

For frequency band $\mathbb{B}_{sub}$, which is highly sensitive to uncertainties, it is seen that an increasing of the mass and elastic uncertainty level yield a small spread around the secondary resonance accompanied by a moderate inhibition of the response level. In summary, the geometric nonlinear effects seem to mainly act on the uncertainty propagation by spreading the response on the whole band of analysis without drastically amplifying the amplitude of the main resonance. The main drastic consequence of such result mainly concerns the sub-frequency band $\mathbb{B}_{sub}$ for which the geometric nonlinearities act as an intrinsic excitation, yielding secondary

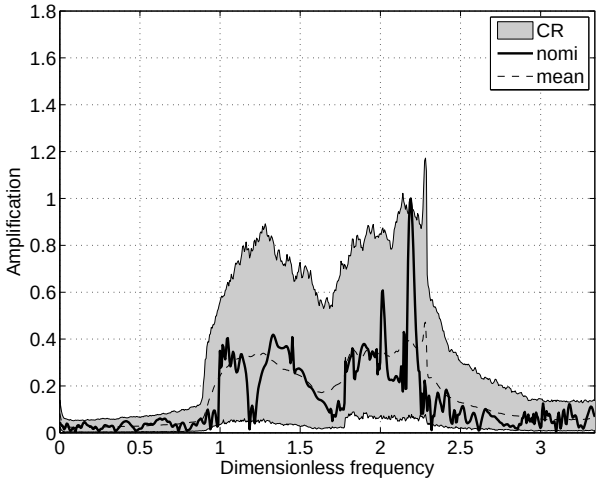

Figure 12: Stochastic analysis: frequency domain observation $Y^{NL}(2\pi\nu)$ related to the nonlinear case when $\delta_K = \delta_M = 0.16$ and $\delta_{K_c} = \delta_C = \delta_D = 0.2$: mean model (thick line), mean of the stochastic model (thin dashed line), confidence region (gray region).

resonances. The wide spread of uncertainties through a large bandwidth give rise to drastic amplifications with respect to these secondary resonances.

For $\nu/\nu_0 \in \mathbb{B}$, let Y_∞ be the random magnification factor defined by $Y_\infty = \max_{\nu/\nu_0 \in \mathbb{B}} Y(2\pi\nu)$. We then define the second random magnification factor Z_∞ such that

$$Z_\infty = \frac{\max_{\nu/\nu_0 \in \mathbb{B}_{sub}} W(2\pi\nu)}{\max_{\nu/\nu_0 \in \mathbb{B}_{sub}} w(2\pi\nu)} \quad . \tag{6}$$

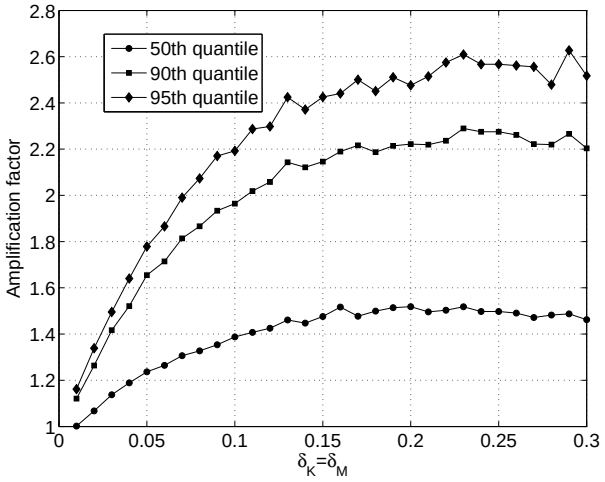

Figure 13: Quantile analysis of magnification factor Y_∞^L with respect to mistuning level δ with $P_C \in \{0.5\,,\, 0.9\,,\, 0.95\}$

Figures 13 displays the graph of the quantiles of Y_∞^L with respect to mistuning rate δ. This latter graph displays a strong sensitivity of the random magnification factor to uncertainties, exhibiting a maximum from which robustness areas limiting the amplification phenomenon can be defined. Figure 13 compares the similar graphs obtained with random observations Y_∞^{NL} and Z_∞^{NL}. Taking into account the geometric nonlinear

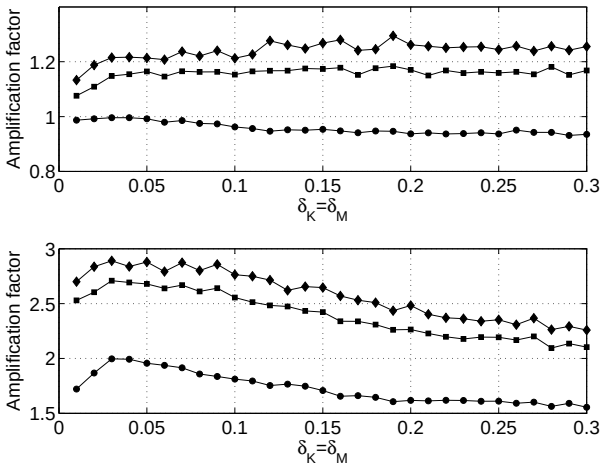

Figure 14: Quantile analysis of magnification factors Y_{∞}^{NL} (upper graph) and Z_{∞}^{NL} (lower graph) with respect to mistuning level δ with $P_C \in \{0.5\,,\ 0.9\,,\ 0.95\}$.

effects yield a drastic decrease of such amplification phenomenon, exhibiting also a limited sensitivity to uncertainties. Nevertheless, a special attention must be given to observation Z_{∞}^{NL}, which points out not only its complex sensitivity to uncertainties but also high amplification levels, that may lead to unexpected amplifications of resonances.

Conclusion

The paper has presented an analysis of the geometrical nonlinear effects of an uncertain mistuned rotating industrial integrated bladed disk subjected to a high loading level. Firs of all, a nonlinear dynamic analysis of the tuned structure has allowed the effects of the geometric nonlinearities to be characterized in both the time domain and the frequency domain. The dynamical response of the blades has also been investigated outside the frequency domain of excitation. The linear response has its energy concentrated in the frequency domain of excitation whereas a more complex dynamical situation is observed in the nonlinear geometrical case. It has been seen that the nonlinear response is spread all outside the frequency band of excitation, yielding secondary resonances with magnitudes comparable with the main resonance. A nonlinear analysis of the mistuned structure has then been proposed. Compared with the linear mistuned case, the nonlinear mistuned response predictions yield low vibration amplitudes. Nevertheless, for a given mistuning rate, the nonlinear mistuned response predictions are much more robust to uncertainties in the frequency band of excitation. One notable result is that the geometrical nonlinearities widely propagate the uncertainties outside the frequency band of excitation, giving rise to broad confidence regions in the low frequencies. A complex vibratory situation is observed with the apparition of unexpected secondary resonances, highly sensitive to uncertainties. Those resonances are not excited through the loading but through the geometric nonlinearities.

Acknowledgements

This work was supported by the DGA (French defence procurement agency) in the context of the TURBO-DYNA project (project number ANR-13-ASTR-0008-01) related to the ANR ASTRID research program (specific support scheme for research works and innovation defence). SAFRAN Turbomeca is also acknowledged for giving permission to publish this work.

References

[1] S.-T. Wei and C. Pierre, *Localization Phenomena in Mistuned Assemblies with Cyclic Symmetry Part II: Forced Vibrations*, ASME Journal of Vibration, Acoustics Stress and Reliability in Design, Vol. 110(4), (1988) pp. 439-449.

[2] R. Bladh, M.-P. Castanier, C. Pierre, *Component-mode-based reduced-order modeling techniques for mistuned bladed disks - Part I: Theoretical models*, ASME Journal of Engineering Gas, Turbine and Power, Vol.123(1), (2001), pp. 89-99.

[3] M. Mbaye, C. Soize, J. Ousty, *A reduced-order model of detuned cyclic dynamical systems with geometric modifications using a basis of cyclic modes*, ASME Journal of Engineering for Gas Turbines and Power, Vol.132(11), (2010), paper 112502.

[4] A.-J. Rivas-Guerra, M.-P. Mignolet, J.-P. Delor, *Identification of mistuning characteristics of bladed disks from free response data - Part II*, ASME Journal of Engineering Gas, Turbine and Power, Vol.123(2), (2001), pp. 404-411.

[5] M. Mbaye, C. Soize, J. Ousty, E. Capiez-Lernout, *Robust Analysis of Design in Vibration of Turbomachines*, ASME Journal of Turbomachinery, Vol.135(2), (2013), paper 021008.

[6] E. Capiez-Lernout, C. Soize, *Nonparametric modeling of random uncertainties for dynamic response of mistuned bladed disks*, ASME Journal of Engineering Gas, Turbine and Power, Vol.126(3), (2004), pp. 610-618.

[7] A.F. Vakakis, *Dynamics of a nonlinear periodic structure with cyclic symmetry*, Acta Mechanica, Vol.95(1-4), (1992), pp. 197-226.

[8] A. Grolet, F. Thouverez, *Vibration analysis of a nonlinear system with cyclic symmetry*, ASME Journal of Engineering for Gas Turbines and Power, Vol.133(2), (2011), paper 022502.

[9] E. Capiez-Lernout, C. Soize, M.-P. Mignolet, *Post-buckling nonlinear static and dynamical analyses of uncertain cylindrical shells and experimental validation* Computer Methods in Applied Mechanics and Engineering, Vol. 271, (2014), pp. 210-230.

[10] M.-P. Mignolet, A. Przekop, S.A. Rizzi, M.S. Spottswood, *A review of indirect/non-intrusive reduced-order modeling of nonlinear geometric structures*, Journal of Sound and Vibration, Vol.332(10), (2013), pp.2437-2460.

[11] C. Soize, *Stochastic Models of Uncertainties in Computational Mechanics*, Lecture Notes in Engineering Mechanics 2, American Society of Civil Engineers (ASCE) (2012).

[12] C. Soize, *Random matrix theory for modeling uncertainties in computational mechanics*, Computer Methods in Applied Mechanics and Engineering, Vol. 194(12-16), (2005), pp. 1333-1366.

[13] A.A. Muryavov, S.A. Rizzi, *Determination of nonlinear stiffness with application to random vibration of geometrically nonlinear structures*, Computers and Structures, Vol.81, (2003), pp.1513-1523.

[14] E. Capiez-Lernout, C. Soize, M.-P. Mignolet, *Computational stochastic statics of an uncertain curved structure with geometrical nonlinearity in three-dimensional elasticity* Computational Mechanics, Vol. 49(1), (2012), pp. 87-97.

[15] M. Mignolet, C. Soize, *Stochastic reduced-order models for uncertain geometrically nonlinear dynamical systems*, Computer Methods in Applied Mechanics and Engineering, Vol. 197, (2008), pp. 3951-3963.

[16] M.A. Crisfield, *nonlinear finite element analysis of solids and structures, Vol. 1 : essentials*, John Wiley and Sons, Chichester (1997).

[17] C. Soize, *Medium frequency linear vibrations of anisotropic elastic structures.*, La recherche aérospatiale (english version), Vol.5, (1982), pp.65-87.

[18] D.L. Thomas, *Dynamics of rotationnally periodic structures*, International Journal for Numerical Methods in Engineering, Vol. 14, (1979), pp. 81-102.

[19] A. Bossavit, *Boundary value problems with symmetry and their approximation by finite elements*, SIAM Journal of Applied Mathematics, Vol. 53, No. 5, (1993), pp.1352-1380.